

Journal of Materials Chemistry A

Accepted Manuscript



This is an *Accepted Manuscript*, which has been through the Royal Society of Chemistry peer review process and has been accepted for publication.

Accepted Manuscripts are published online shortly after acceptance, before technical editing, formatting and proof reading. Using this free service, authors can make their results available to the community, in citable form, before we publish the edited article. We will replace this *Accepted Manuscript* with the edited and formatted *Advance Article* as soon as it is available.

You can find more information about *Accepted Manuscripts* in the [Information for Authors](#).

Please note that technical editing may introduce minor changes to the text and/or graphics, which may alter content. The journal's standard [Terms & Conditions](#) and the [Ethical guidelines](#) still apply. In no event shall the Royal Society of Chemistry be held responsible for any errors or omissions in this *Accepted Manuscript* or any consequences arising from the use of any information it contains.

Thermoelectric properties of the $\text{Yb}_9\text{Mn}_{4.2-x}\text{Zn}_x\text{Sb}_9$ solid solution

Saneyuki Ohno¹, Alexandra Zevalkink^{1,3}, Yoshiki Takagiwa², Sabah K. Bux³, G. Jeffrey Snyder¹

¹Materials Science, California Institute of Technology, 1200 E. California Blvd., Pasadena, CA 91125

²Department of Advanced Materials Science, The University of Tokyo, Kiban-toh 502, 5-1-5 Kashiwanoha, Kashiwa-shi, Chiba 277-8561

³Thermal Energy Conversion Technologies Group, Jet Propulsion Laboratory, California Institute of Technology, 4800 Oak Grove Drive, MS 277-207, Pasadena, CA 91109

ABSTRACT

$\text{Yb}_9\text{Mn}_{4.2}\text{Sb}_9$ has been shown to have extremely low thermal conductivity and a high thermoelectric figure of merit attributed to its complex crystal structure and disordered interstitial sites. Motivated by previous work showing that isoelectronic substitution of Mn by Zn leads to higher mobility by reducing spin disorder scattering, this study investigates the thermoelectric properties of the solid solution $\text{Yb}_9\text{Mn}_{4.2-x}\text{Zn}_x\text{Sb}_9$ ($x = 0, 1, 2, 3$ and 4.2). Measurements of the Hall mobility at high temperature (up to 1000 K) show that the mobility can be increased by more than a factor of 3 by substituting Zn into Mn sites. This increase is explained by the reduction of the valence band effective mass with increasing Zn, leading to a slightly improved thermoelectric quality factor relative to $\text{Yb}_9\text{Mn}_{4.2}\text{Sb}_9$. However, increasing the Zn-content also increases the p -type carrier concentration, leading to metallic behavior with low Seebeck coefficients and high electrical conductivity. Varying the filling of the interstitial site in $\text{Yb}_9\text{Zn}_{4+y}\text{Sb}_9$ ($y = 0.2, 0.3, 0.4$ and 0.5) was attempted, but the carrier concentration ($\sim 10^{21} \text{ cm}^{-3}$ at 300K) and Seebeck coefficients remained constant, suggesting that the phase width of $\text{Yb}_9\text{Zn}_{4+y}\text{Sb}_9$ is quite narrow.

INTRODUCTION

Solid-state thermoelectric generators would be an ideal clean and reliable source of energy harvesting system due to their ability to generate electricity directly from waste heat. For the purpose of widespread applications, it is necessary to improve the efficiency of thermoelectric materials, quantified by the thermoelectric figure of merit ($zT = \alpha^2 T / \kappa \rho$).¹ A good thermoelectric material must strike a balance between a large Seebeck coefficient (α), low electrical resistivity (ρ), and low total thermal conductivity (κ), all of which are related via the free majority carrier concentration (n).² Here, the total thermal conductivity is a combination of electronic thermal conductivity (κ_{el}) and lattice thermal conductivity (κ_L).

Zintl compounds provide many of the characteristics required for good thermoelectric materials.³ Zintl phases are made up of electropositive cations that donate their electrons to anions, which in turn must form covalent bonds to satisfy valence.^{5,6} They often have very low lattice thermal conductivity due to their large unit cells, and it is possible to finely tune their electronic properties by doping, providing a route to improved zT . High thermoelectric efficiency has been demonstrated in a number of different Zintl compounds⁷⁻¹⁷ including $\text{Yb}_{14}\text{MnSb}_{11}$ ^{16, 18} and $\text{YbCd}_{2-x}\text{Zn}_x\text{Sb}_2$, both of which have zT values above unity at high temperatures.^{11, 19-36}

Recently, $\text{Yb}_9\text{Mn}_{4.2}\text{Sb}_9$ was shown by Bux et al. to have promising thermoelectric performance ($zT = 0.7$ at 950K)¹⁷. The structure of $\text{Yb}_9M_{4+x}\text{Sb}_9$ is shown in Figure 1, where M can be either Mn^{2+} , Cd^{2+} or Zn^{2+} .^{37, 38} Although this structure type was originally discovered in 1970's,³⁹ the interstitial site was not recognized until 2004 by Bobev et al.³⁸ The structure contains ribbons of MSb_4 tetrahedra that are connected by partially occupied interstitial M sites. The $\text{Yb}_9M_{4+x}\text{Sb}_9$ structure would be charge balanced based on a simple electron counting rules if the interstitial M sites were 25% occupied, corresponding to $x = 0.5$. In practice, the Mn

analogue, $\text{Yb}_9\text{Mn}_{4+x}\text{Sb}_9$, was found to behave as a line compound with approximately 10% occupation of the interstitial sites ($x = 0.2$).^{17, 37} In the Zn-containing analogue, the exact composition is unclear, as the literature reports four different stoichiometries ($\text{Yb}_9\text{Zn}_{4.18}\text{Sb}_9$, $\text{Yb}_9\text{Zn}_{4.23}\text{Sb}_9$, $\text{Yb}_9\text{Zn}_{4.380}\text{Sb}_9$ and $\text{Yb}_9\text{Zn}_{4.384}\text{Sb}_9$) determined from refinement of single crystal X-ray diffraction data.^{37, 38}

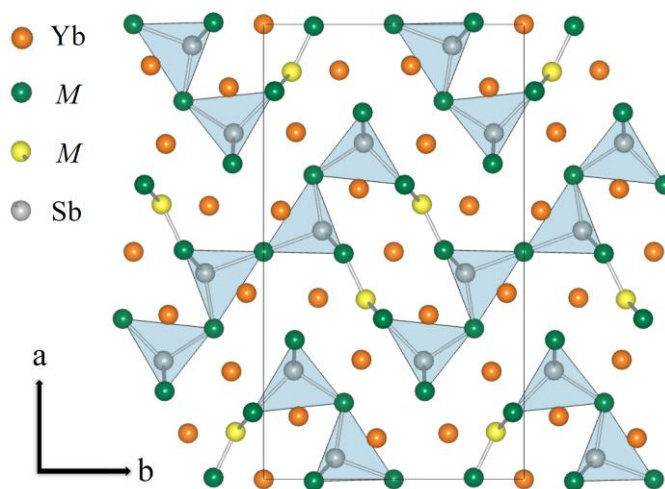


Figure 1. The $\text{Yb}_9\text{M}_{4+x}\text{Sb}_9$ structure contains infinite M_4Sb_9 “ribbons” made up of corner sharing MSb_4 tetrahedra, where M is a 2+ transition metal that can be either Mn, Cd or Zn.^{37, 38} Partially occupied M -interstitial sites (yellow spheres) link neighboring M_4Sb_9 ribbons into a pseudo two-dimensional framework.

The high zT reported for $\text{Yb}_9\text{Mn}_{4.2}\text{Sb}_9$ stems from its low, glass-like lattice thermal conductivity ($\kappa_L \approx 0.5$ W/mK at room temperature) and optimized electronic properties¹⁷. To improve zT further, it is thus necessary to improve the inherent electronic properties of this system by tuning either the band structure or carrier scattering. One potential route is to increase the carrier mobility by substituting Zn on the Mn site, as demonstrated in the $\text{YbZn}_{2-x}\text{Mn}_x\text{Sb}_2$ and $\text{Yb}_{14}\text{Mn}_{1-x}\text{Zn}_x\text{Sb}_9$ solid solutions.^{7, 13} In $\text{YbZn}_{2-x}\text{Mn}_x\text{Sb}_2$, the mobility of the Zn end-member is much higher than that of the Mn end-member, even though the effective mass remains unchanged. Similarly, in $\text{Yb}_{14}\text{Mn}_{1-x}\text{Zn}_x\text{Sb}_{11}$, increased Zn content leads to improved mobility. In both cases, the substitution of Zn leads to improved thermoelectric performance. These results

motivate the current investigation of the thermoelectric properties of the $\text{Yb}_9\text{Mn}_{4.2-x}\text{Zn}_x\text{Sb}_9$ solid solution ($x = 0, 1, 2, 3$ and 4.2).

RESULTS AND DISCUSSION

Synthesis and Characterization. $\text{Yb}_9\text{Mn}_{4.2-x}\text{Zn}_x\text{Sb}_9$ ($x = 0, 1, 2, 3$ and 4.2) and $\text{Yb}_9\text{Zn}_{4+y}\text{Sb}_9$ ($y = 2, 3, 4$ and 5) samples were prepared by ball milling followed by hot pressing (details are described in the Experimental section). To characterize these samples, X-ray diffraction (XRD) was performed on the polycrystalline slices at room temperature. Figure 2 shows the XRD results for all of the $\text{Yb}_9\text{Mn}_{4.2-x}\text{Zn}_x\text{Sb}_9$ samples ($x = 0, 1, 2, 3$ and 4.2). For the $x = 4.2$ sample, the Rietveld fit and residual are shown as red curves and blue curves respectively. Table 1 shows lattice parameters for solid solutions. As the amount of Zn increases, each lattice parameter varies linearly, in agreement with previously reported results.^{37, 38} Scanning electron microscopy confirmed that the phase purity of the Zn-containing samples is approximately 95% and revealed YbM_2Sb_2 ($M=\text{Zn}$ or Mn) as a secondary phase.

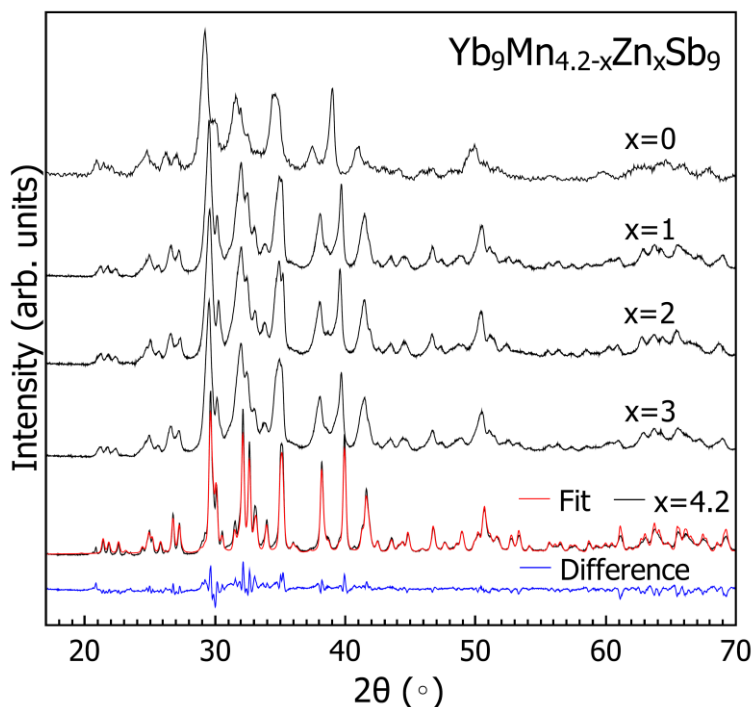


Figure 2. X-ray diffraction patterns for $\text{Yb}_9\text{Mn}_{4.2-x}\text{Zn}_x\text{Sb}_9$ ($x = 0, 1, 2, 3$ and 4.2) samples exhibit no significant impurity phases. The Rietveld fit and difference profile are shown for the Zn end-member.

Table 1. Lattice parameters for $\text{Yb}_9\text{Mn}_{4.2-x}\text{Zn}_x\text{Sb}_9$ were calculated from XRD results using Rietveld fits. As the amount of Zn increases, each parameter changes linearly from the Mn end member side to Zn end member and this follows the reported trend.^{37, 38}

Composition	a (Å)	b (Å)	c (Å)
x = 0	22.014	12.231	4.6079
x = 1	21.834	12.327	4.5841
x = 2	21.764	12.334	4.5664
x = 3	21.711	12.343	4.5451
x = 4.2	21.692	12.409	4.5278

Electronic transport properties The electronic transport properties of $\text{Yb}_9\text{Mn}_{4.2-x}\text{Zn}_x\text{Sb}_9$ ($x = 0, 1, 2, 3$ and 4.2) samples are shown in Figure 3 and 4. The Mn analogue, $\text{Yb}_9\text{Mn}_{4.2}\text{Sb}_9$, is a line compound with an electron deficient composition, resulting in a carrier concentration of $4 \times 10^{20} \text{ h}^+/\text{cm}^3$ and degenerate semiconducting behavior. Surprisingly, considering that Zn and Mn both have the same valence state in this structure, substituting Zn on the Mn site increases

the carrier concentration (n_H) sharply, as shown in Figure 3a. Using simple electron counting rules, a carrier concentration of $n_H = 0 \text{ h}^+/\text{cm}^3$ corresponds to 25% occupation of the interstitial sites ($\text{Yb}_9\text{M}_{4.5}\text{Sb}_9$), while completely empty interstitial sites ($\text{Yb}_9\text{M}_{4.0}\text{Sb}_9$) yield $n_H = 1.66 \times 10^{21} \text{ h}^+/\text{cm}^3$. Thus, the higher n_H in Zn-containing samples may indicate that the solubility of Zn on the interstitial sites is lower than that of Mn. Additionally, in the Zn containing samples, n_H decreases by nearly an order of magnitude as the temperature increases. Both of these effects may be because introducing Zn changes the defect chemistry by lowering the energy to form acceptor defects.³⁵

The Hall mobility (μ_H) of $\text{Yb}_9\text{Mn}_{4.2-x}\text{Zn}_x\text{Sb}_9$ samples (Figure 3c) decreases with temperature as expected when acoustic phonons are the primary scattering source. The change in μ_H as a function of Zn content at 300 K is shown in Figure 3d. The mobility of the Zn end-member is increased by a factor of three relative to the Mn analogue. The slight reduction at intermediate values of x is due to the disorder on the transition metal site.⁴⁰

Increased mobility can arise from either increased carrier relaxation time (τ) or decreased effective mass (m^*). When acoustic phonon scattering controls the mobility, the scattering rate $\frac{1}{\tau(k)}$ is determined by the acoustic deformation potential (Ξ), acoustic phonon velocity (v_s), density (ρ), and the density of states ($g(E)$).⁴¹

$$\frac{1}{\tau(k)} = \frac{k_B T \Xi^2 \pi g(E)}{\hbar v_s^2 \rho} \quad (1)$$

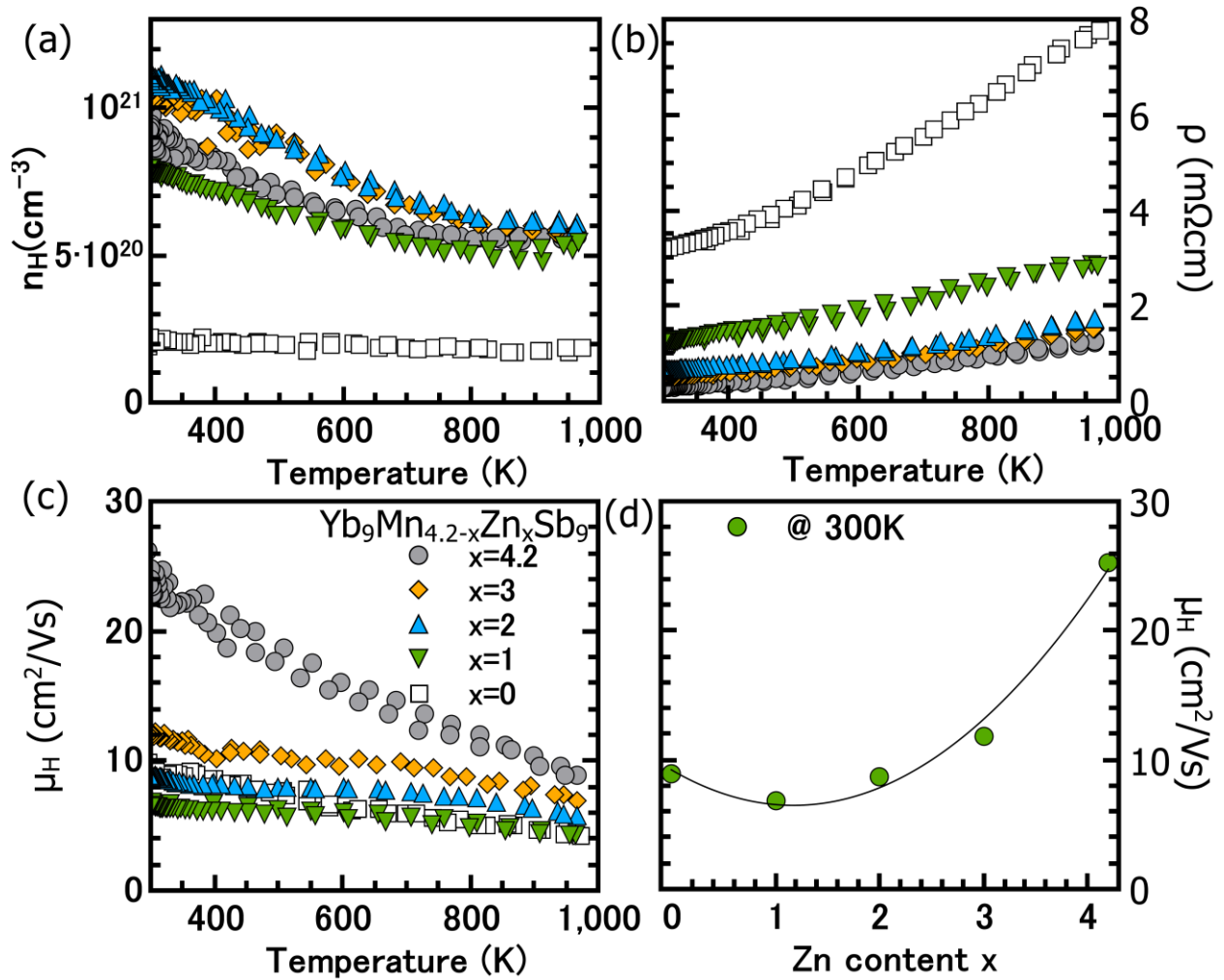


Figure 3. With increasing Zn content, x , the (a) Hall carrier concentration of $\text{Yb}_9\text{Mn}_{4.2-x}\text{Zn}_x\text{Sb}_9$ samples increases and (b) the resistivity decreases. (c) The Hall mobility decreases with temperature due to acoustic phonon scattering. (d) As a function of x at 300 K, the mobility decreases due to alloy scattering and then rises sharply with complete substitution of Mn by Zn.

Substituting the density of states in three dimensions ($g_{3D}(E) = \frac{1}{2\pi^2} \left(\frac{2m^*}{\hbar^2}\right)^{3/2} \sqrt{E}$) into Eq.1,

yields the following relationship which shows that τ is also dependent on effective mass in this

case.

$$\tau \propto \frac{1}{(m^*)^{3/2}} \quad (2)$$

Inserting Eq 2 into the expression for mobility, the following proportionality is acquired for mobility limited by acoustic phonon scattering.

$$\mu \propto \frac{\tau}{m^*} \propto \frac{1}{(m^*)^{5/2}} \quad (3)$$

The Seebeck coefficients (α) of $\text{Yb}_9\text{Mn}_{4.2-x}\text{Zn}_x\text{Sb}_9$ ($x = 0, 1, 2, 3$ and 4.2) samples are shown as a function of temperature and carrier concentration in Figures 4a and b, respectively. The Seebeck coefficients decrease as the amount of Zn, and thus the carrier concentration, increases. However the decrease in α is much greater than should be expected if m^* is unchanged. From the experimental Seebeck coefficients, the chemical potentials (η) at 975K are calculated within a single parabolic band (SPB)¹⁰ model using Eq.4 with $\lambda = 0$ (acoustic-phonon scattering), where $F_j(\eta)$ is the Fermi integral given in Eq 6. The hole effective masses for the pure Zn and pure Mn samples ($0.65 m_e$ and $1.2 m_e$, respectively), determined from Eq 5 using the experimental n_H , were used to generate the dashed curved shown in Figure 4b.

$$\alpha = \frac{k}{e} \left(\frac{(2+\lambda)F_{1+\lambda}(\eta)}{(1+\lambda)F_\lambda(\eta)} - \eta \right) \quad (4)$$

$$n = 4\pi \left(\frac{2m^*kT}{h^2} \right)^{3/2} F_{1/2}(\eta) \quad (5)$$

$$F_j(\eta) = \int_0^\infty \frac{\zeta^j d\zeta}{1+\text{Exp}[\zeta-\eta]} \quad (6)$$

From Eq 3, we can see that the observed difference in m^* can fully explain the difference in mobility between the Mn and Zn analogues of the $\text{Yb}_9\text{M}_{4.2}\text{Sb}_9$ structure. An increased τ due to reduced spin disorder scattering is thus not necessary to explain the increased mobility in this case. This is in contrast to the $\text{YbZn}_{2-x}\text{Mn}_x\text{Sb}_2$ system, in which m^* remained constant, and τ increased upon Zn substitution.

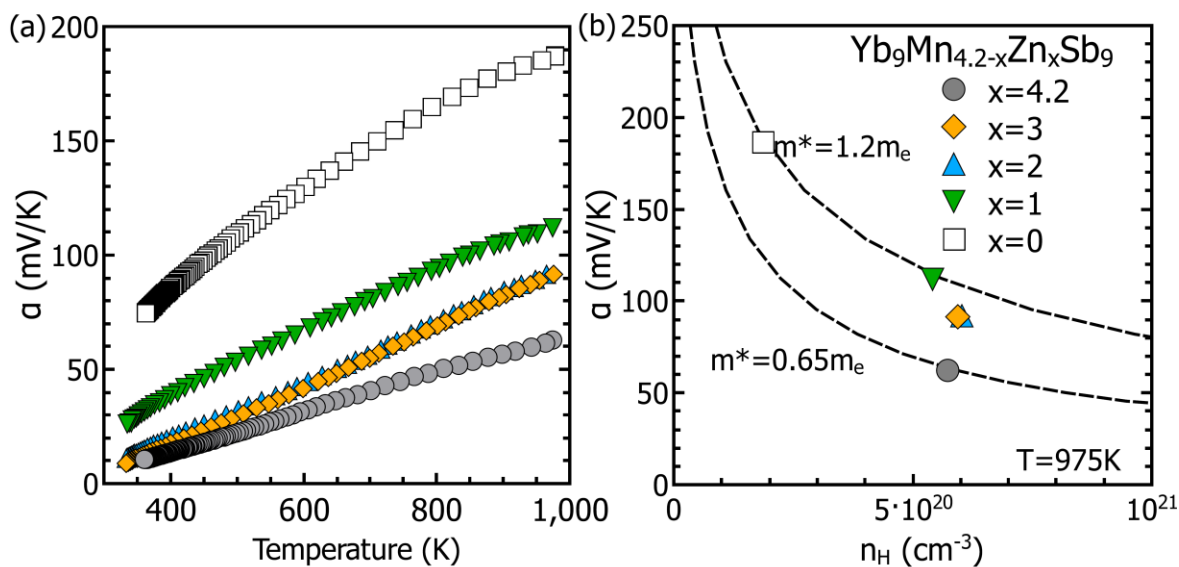


Figure 4. (a) The Seebeck coefficients of $\text{Yb}_9\text{Mn}_{4.2-x}\text{Zn}_x\text{Sb}_9$ ($x=0, 1, 2, 3$ and 4.2) samples are consistent with degenerate semiconducting behavior. (b) The dashed curves, calculated with an SPB model using the parameters shown in Table 4, indicate that m^* is decreasing as the amount of Zn is increased.

Thermal transport properties Shown in Figure 5a, the total thermal conductivity (κ_{total}) for $\text{Yb}_9\text{Mn}_{4.2-x}\text{Zn}_x\text{Sb}_9$ samples was calculated from the measured thermal diffusivity D using $\kappa_{\text{total}} = DdC_p$, where d is the geometric density and C_p is the Dulong Petit heat capacity. In Zn-containing samples, κ_{total} is higher than in the Mn end-member due to the dominance of the electronic contribution. The lattice component (κ_L) of the thermal conductivity was obtained by subtracting the electronic component (κ_{el}), calculated via the Wiedemann-Flanz law from the total thermal conductivity ($\kappa_{el} = LT\sigma$, where L and σ are the Lorenz number and electrical conductivity, respectively). Often, L is calculated as a function of temperature using an SPB model, thus falling in between the non-degenerate and degenerate limits (1.5 and 2.4, respectively). Using an SPB model yields a lattice thermal conductivity (Figure 5b) for $\text{Yb}_9\text{Mn}_{4.2}\text{Sb}_9$ that is near the minimum theoretical value (κ_{min}), defined by Eq (7).

$$\kappa_{\min} = \frac{1}{2} \left(\frac{\pi}{6} \right)^{\frac{1}{3}} k_B V^{-\frac{2}{3}} (2v_T + v_L) \quad (7)$$

Here, V , v_T , and v_L are the average volume per atom, the transverse speed of sound, and longitudinal speed of sound respectively.^{17,42} Room temperature ultrasonic measurements of the Zn end-member show that v_T , and v_L are comparable to the Mn analogue, as shown in Table 2, suggesting that the Zn- and Mn-based samples should have similar values of κ_L ¹⁷. However, in the Zn-containing samples, an SPB model yields unrealistically high values of L , and thus underestimates κ_L . Thus, in Figure 5b, rather than using an SPB model for L in the Zn-containing samples, we use L as a temperature-independent “fitting parameter” by setting $\kappa_L = \kappa_{\min}$ at 923 K. The resulting values of L are given in Table 3. Note that the use of a temperature-independent L for the Zn-containing samples leads to slightly overestimated values of κ_L at lower temperatures.

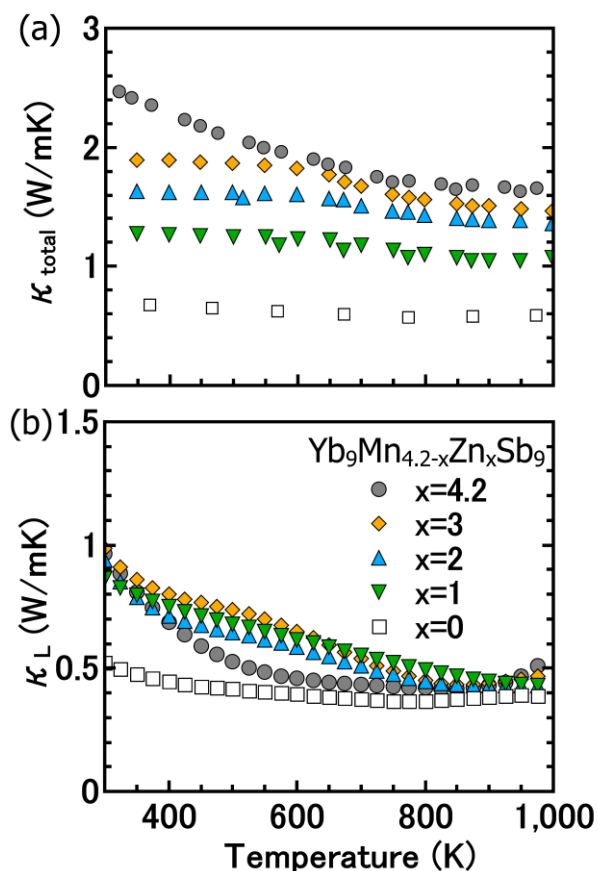


Figure 5. (a) The total thermal conductivity of $\text{Yb}_9\text{Mn}_{4.2-x}\text{Zn}_x\text{Sb}_9$ ($x = 0, 1, 2, 3$ and 4.2) increases with x . (b) The lattice thermal conductivity was estimated for Zn-containing samples using the temperature independent Lorenz numbers given in Table 3.

Table 2. Room temperature ultrasonic measurements: shows that the longitudinal and transverse speeds of sound Zn compound are slightly higher than the Mn analogue.

Speed of Sound	Longitudinal	Transverse
$\text{Yb}_9\text{Zn}_{4.2}\text{Sb}_9$	3228 m/s	1920 m/s
$\text{Yb}_9\text{Mn}_{4.2}\text{Sb}_9$	3070 m/s	1730 m/s

Table 3. Lorenz numbers were obtained by setting the minimum experimental lattice thermal conductivities to the calculated theoretical minimum. For the pure Mn sample, L was calculated using an SPB model as shown in ref 13.

Composition	Lorenz number ($\times 10^{-8} \cdot \text{W} \cdot \Omega \cdot \text{K}^{-2}$)
$x = 1$	1.77
$x = 2$	1.61
$x = 3$	1.70
$x = 4.2$	1.50

Varying interstitial Zn content Although the mobility of $\text{Yb}_9\text{Zn}_4\text{Sb}_9$ is three times higher than that of the Mn analogue, the carrier concentration is higher than typically desired for thermoelectric applications. In an attempt to control the carrier concentration by increasing the interstitial Zn concentration, we synthesized $\text{Yb}_9\text{Zn}_{4+y}\text{Sb}_9$ samples with $y = 0.2, 0.3, 0.4$ and 0.5 . However, Hall measurements indicate that the carrier concentration remains constant ($n_{\text{H}} \sim 10^{21} \text{ h}^+/\text{cm}^3$) as the amount of Zn added synthetically is varied (Figure 6a). The Seebeck coefficients, shown in Figure 6b, also remain nearly constant as a function of synthetic Zn content, suggesting that the composition range of $\text{Yb}_9\text{Zn}_{4+y}\text{Sb}_9$ may be quite narrow, similar to that of the Mn analogue.

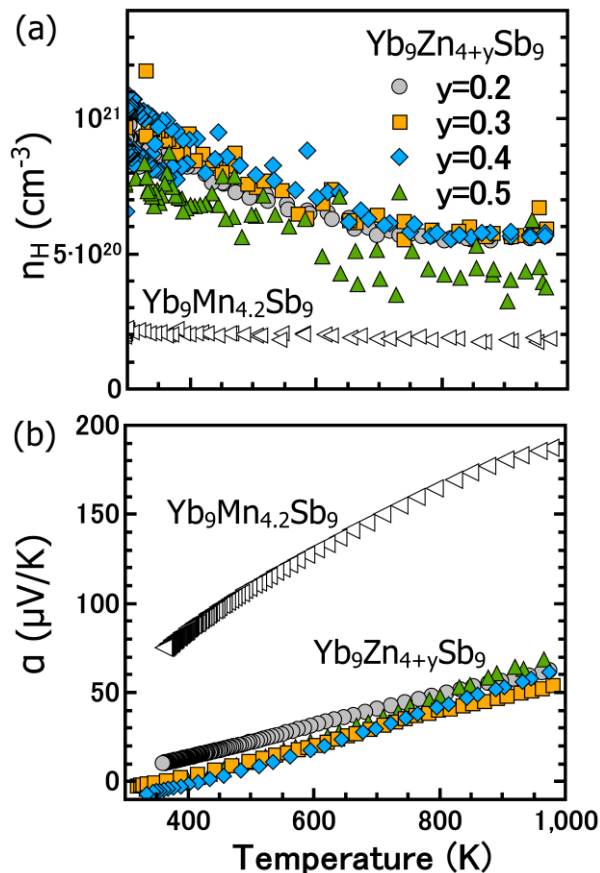


Figure 6. (a) The carrier concentration remains unchanged in samples with synthetic compositions of $\text{Yb}_9\text{Zn}_{4+y}\text{Sb}_9$ ($y=2, 3, 4$ and 5). (b) The Seebeck coefficients are also unaffected by varying the synthetic Zn content.

Figure of Merit Figure 7 shows the experimental zT of $\text{Yb}_9\text{Mn}_{4.2-x}\text{Zn}_x\text{Sb}_9$ solid solution samples ($x = 0, 1, 2, 3, 4.2$) as a function of carrier concentration at 975 K. An SPB model was used to predict the figure of merit as a function of n for the $\text{Yb}_9\text{Mn}_{4.2}\text{Sb}_9$ and $\text{Yb}_9\text{Zn}_{4.2}\text{Sb}_9$ end-members (shown as dashed curves) using the parameters in Table 4. The lower effective mass and higher mobility in the Zn analogue shift the optimal carrier concentration downwards relative to $\text{Yb}_9\text{Mn}_{4.2}\text{Sb}_9$. The predicted maximum figure of merit is somewhat higher for the Zn analogue due to its higher weighted mobility ($\mu_0(m^*/m_e)^{3/2}$) and dimensionless quality factor^{43, 44} ($B =$

$$\left(\frac{k_B}{e}\right)^2 \frac{2e(k_B T)^{3/2}}{(2\pi)^{3/2} \hbar^3} \frac{\mu_0(m^*/m_e)^{3/2}}{\kappa_L} T, \text{ where } \mu_0 \text{ is an intrinsic mobility calculated by following equation}$$

when charge carriers are scattered by acoustic phonons: $\mu_H = \mu_0 \frac{F_{-1/2}(\eta)}{2F_0(\eta)}$. However, the experimental zT of Zn containing samples is far lower than that of the Mn end-member, due to their high carrier concentrations. While the carrier concentration of $\text{Yb}_9\text{Mn}_{4.2}\text{Sb}_9$ is very close the optimal value, samples with Zn have carrier concentrations that are far too large. However, if it is possible to reduce the carrier concentration of Zn-containing samples by doping with an n -type dopant,^{16, 18} higher zT than that of Mn analogue could potentially be realized in future work.

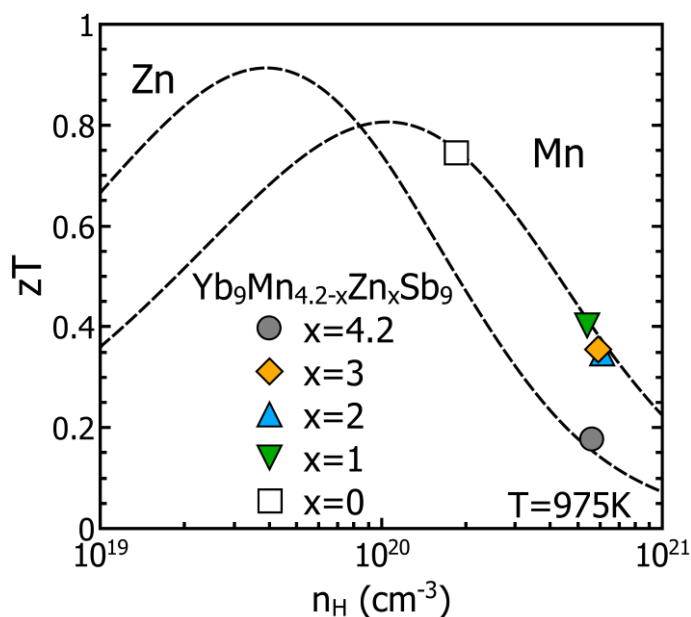


Figure 7. The figure of merit of $\text{Yb}_9\text{Mn}_{4.2-x}\text{Zn}_x\text{Sb}_9$ samples decreases with increasing carrier concentration and Zn content. An SPB model predicts an optimized zT of 0.9 in the Zn system at $n_H = 4 \times 10^{19} \text{ h}^+/\text{cm}^3$.

Table 4. The parameters for the SPB model at 975K.

	$\text{Yb}_9\text{Zn}_{4.2}\text{Sb}_9$	$\text{Yb}_9\text{Mn}_{4.2}\text{Sb}_9$
Effective mass, m^*	0.65 m_e	1.2 m_e
Intrinsic mobility, μ_0	18.65 cm^2/Vs	5.71 cm^2/Vs
Weighted mobility, $\mu_0 (m^*/m_e)^{3/2}$	9.77 cm^2/Vs	7.51 cm^2/Vs
Lattice thermal conductivity, κ_L	0.43 W/mK	0.39 W/mK
Quality factor, B	0.387	0.328

CONCLUSION

The Zintl compound $\text{Yb}_9\text{Mn}_{4.2}\text{Sb}_9$ is a promising thermoelectric material due to its low, glasslike lattice thermal conductivity, essential for high zT . In this research, the effect of substituting Zn on the Mn site in $\text{Yb}_9\text{Mn}_{4.2-x}\text{Zn}_x\text{Sb}_9$ was investigated. Pursuing this strategy led to a factor of two reduction in the valence band mass, and thus increased carrier mobility and decreased Seebeck coefficients. The thermoelectric quality factor of the $\text{Yb}_9\text{Mn}_{4.2-x}\text{Zn}_x\text{Sb}_9$ system was found to be somewhat higher in the Zn analogue due to its improved mobility. However, the carrier concentration in Zn-containing samples was too high, and varying the synthetic Zn content did not lead to desired carrier concentration control. In future studies, *n*-type dopants might be able to be used to reduce the carrier concentration and achieve a higher figure of merit.

EXPERIMENTAL

$\text{Yb}_9\text{Mn}_{4.2-x}\text{Zn}_x\text{Sb}_9$ ($x=0, 1, 2, 3$ and 4.2) and $\text{Yb}_9\text{Zn}_{4+y}\text{Sb}_9$ ($y=2, 3, 4$ and 5) samples were prepared by ball milling followed by hot pressing. The elements were loaded into stainless-steel vials with stainless-steel balls inside the glove box filled with argon. The materials were dry ball-milled for an hour using a SPEX Sample Prep 8000 Series mixer/mill. The fine powder was hot-pressed in high-density graphite dies using 40 MPa on a 12 mm diameter surface. Samples were hot pressed using a maximum temperature of 1073 K for 2 hours under flowing argon, followed by 2 hour cooling. To determine the phase purity of the products, X-ray diffraction was performed after polishing with a Philips X'Pert MPD diffractometer operated at 45kV and 40mA, and Rietveld analysis was performed using Philips X'part plus software. A Zeiss 1550 VP scanning electron microscope was also used to investigate the phase purity.

For measuring thermoelectric properties, a Netzsch LFA 457 was used to measure thermal diffusivity. Electronic resistivity and Hall coefficient was determined using the 4-point probe Van der Pauw technique with a 0.8 T field under high vacuum.⁴⁵ The Seebeck coefficient was measured using a light-pipe method with tungsten-niobium thermocouples also under high vacuum.⁴⁶

ACKNOWLEDGEMENT

This work was supported by the NASA Science Missions Directorate's Radioisotope Power Systems Technology Advancement Program and Japan Student Service Organization. Y. T. acknowledges support from Sumitomo Foundation (grant no. 120567) and the Murata Science Foundation.

REFERENCES

1. L. E. Bell, *Science*, 2008, **321**, 1457.
2. G. J. Snyder and E. S. Toberer, *Nature Mater.*, 2008, **7**, 105-114.
3. E. S. Toberer, A. F. May and G. J. Snyder, *Chemistry of Materials*, 2010, **22**, 624-634.
4. M. Mills, R. Lam, M. J. Ferguson, L. Deakin and A. Mar, *Coordination Chem. Rev.*, 2002, **233-234**, 207-222.
5. S. M. Kauzlarich, S. R. Brown and G. J. Snyder, *Dalton Trans*, 2007, 2099-2107.
6. S. M. Kauzlarich, *Chemistry, Structure, and Bonding of Zintl Phases and Ions*, Wiley-VCH, 1996.
7. S. Brown, E. S. Toberer, T. Ikeda, C. A. Cox, F. Gascoin, S. Kauzlarich and G. Snyder, *Chem. Mater.*, 2008, **20**.
8. A. Zevalkink, E. S. Toberer, W. G. Zeier, E. Flage-Larsen and G. J. Snyder, *Energy & Environmental Science*, 2011, **4**, 510.
9. W. G. Zeier, A. Zevalkink, E. Schechtel, W. Tremel and G. J. Snyder, *Journal of Materials Chemistry*, 2012, **22**, 9826.
10. E. S. Toberer, A. Zevalkink, N. Crisosto and G. J. Snyder, *Adv. Funct. Mater.*, 2010, **20**, 4375-4380.
11. A. Zevalkink, G. S. Pomrehn, S. Johnson, J. Swallow, Z. M. Gibbs and G. J. Snyder, *Chemistry of Materials*, 2012, **24**, 2091-2098.
12. F. Gascoin, S. Ottensmann, D. Stark, M. S. Haile and G. Snyder, *Adv. Funct. Mater.*, 2005, **15**, 1860-1864.
13. C. Yu, T. J. Zhu, S. N. Zhang, X. B. Zhao, J. He, Z. Su and T. M. Tritt, *J. Appl. Phys*, 2008, **104**, 013705.
14. A. F. May, M. A. McGuire, J. Ma, O. Delaire, A. Huq and R. Custelcean, *Journal of Applied Physics*, 2012, **111**, 033708.
15. K. Guo, Q.-G. Cao, X.-J. Feng, M.-B. Tang, H.-H. Chen, X. Guo, L. Chen, Y. Grin and J.-T. Zhao, *Eu. J. Inorg. Chem.*, 2011, **2011**, 4043-4048.

16. E. S. Toberer, S. R. Brown, T. Ikeda, S. M. Kauzlarich and G. Jeffrey Snyder, *Applied Physics Letters*, 2008, **93**, 062110.
17. S. K. Bux, A. Zevalkink, O. Janka, D. Uhl, S. Kauzlarich, J. G. Snyder and J.-P. Fleurial, *Journal of Materials Chemistry A*, 2014, **2**, 215-220.
18. E. S. Toberer, C. A. Cox, S. R. Brown, T. Ikeda, A. F. May, S. M. Kauzlarich and G. J. Snyder, *Advanced Functional Materials*, 2008, **18**, 2795-2800.
19. X.-J. Wang, M.-B. Tang, H.-H. Chen, X.-X. Yang, J.-T. Zhao, U. Burkhardt and Y. Grin, *Applied Physics Letters*, 2009, **94**, 092106.
20. S. Brown, S. Kauzlarich, F. Gascoin and G. J. Snyder, *Chem. Mater.*, 2006, **18**, 1873-1877.
21. M. Christensen, A. B. Abrahamsen, N. B. Christensen, F. Juranyi, N. H. Andersen, K. Lefmann, J. Andreasson, C. R. Bahl and B. B. Iversen, *Nat Mater*, 2008, **7**, 811-815.
22. A. M. Guloy, R. Ramlau, Z. Tang, W. Schnelle, M. Baitinger and Y. Grin, *Nature*, 2006, **443**, 320-323.
23. I. Bednar, E. Royanian, S. Bühler-Paschen, E. Bauer, N. Nasir, A. Grytsiv, N. Melnychenko-Koblyuk and P. Rogl, *Journal of Electronic Materials*, 2010, **39**, 1687-1691.
24. T. Yi, C. A. Cox, E. S. Toberer, G. J. Snyder and S. M. Kauzlarich, *Chemistry of Materials*, 2010, **22**, 935-941.
25. H. Hua, A. Zevalkink, Z. M. Gibbs, G. J. Snyder and S. Bobev, *Chem. Mater.*, 2012.
26. G. Nolas, G. A. Slack, D. Morelli, T. M. Tritt and A. C. Ehrlich, *J. Appl. Phys*, 1996, **79**.
27. H. Kleinke, *Chemistry of Materials*, 2010, **22**, 604-611.
28. X. Shi, Y. Pei, G. J. Snyder and L. Chen, *Energy & Environmental Science*, 2011, **4**, 4086.
29. S. R. Brown, S. M. Kauzlarich, F. Gascoin and G. Jeffrey Snyder, *Journal of Solid State Chemistry*, 2007, **180**, 1414-1420.
30. Y. Wu, A. P. Litvinchuk, E. S. Toberer, G. J. Snyder, N. Newman, A. Fischer, E. W. Scheidt, W. Scherer and U. Häussermann, *Journal of Applied Physics*, 2012, **111**, 123712.
31. A. Zevalkink, J. Swallow and G. J. Snyder, *Journal of Electronic Materials*, 2012, **41**, 813-818.
32. A. Zevalkink, W. G. Zeier, G. Pomrehn, E. Schechtel, W. Tremel and G. J. Snyder, *Energ. Environ. Sci.*, 2012, **5**, 9121.
33. E. S. Toberer, P. Rauwel, S. Gariel, J. Taftø and G. Jeffrey Snyder, *Journal of Materials Chemistry*, 2010, **20**, 9877.
34. A. May, J.-P. Fleurial and G. Snyder, *Physical Review B*, 2008, **78**.
35. E. S. Toberer, A. F. May, B. C. Melot, E. Flage-Larsen and G. J. Snyder, *Dalton Trans*, 2010, **39**, 1046-1054.
36. A. Prokofiev, A. Sidorenko, K. Hradil, M. Ikeda, R. Svagera, M. Waas, H. Winkler, K. Neumaier and S. Paschen, *Nat Mater*, 2013, **12**, 1096-1101.
37. S.-Q. Xia and S. Bobev, *Chem. Mater.*, 2009, **22**, 840-850.
38. S. Bobev, J. D. Thompson, J. L. Sarrao, M. M. Olmstead, H. Hope and S. M. Kauzlarich, *Inorganic Chemistry*, 2004, **43**, 5044-5052.
39. G. C. E. Brechtel, H. Schäfer, *Z. Naturforsch*, 1979, **34B**, 1229.
40. H. Wang, A. D. LaLonde, Y. Pei and G. J. Snyder, *Advanced Functional Materials*, 2013, **23**, 1586-1596.
41. M. Lundstorm, *Fundamentals of carrier transport 2nd edition*, 2000.
42. D. G. Cahill and R. Pohl, *Ann. Rev. Mater. Sci*, 1988, **39**, 93-121.
43. H. Wang, Y. Pei, A. D. LaLonde and G. J. Snyder, in *Thermoelectric Nanomaterials*, eds. K. Koumoto and T. Mori, Springer, 2013, pp. 3-32.
44. Y. Pei, H. Wang and G. J. Snyder, *Advanced Materials*, 2012, **24**, 6125-6135.
45. K. A. Borup, E. S. Toberer, L. D. Zoltan, G. Nakatsukasa, M. Errico, J. P. Fleurial, B. B. Iversen and G. J. Snyder, *The Review of scientific instruments*, 2012, **83**, 123902.
46. C. Wood, D. Zoltan and G. Stapfer, *Rev. Sci. Instruments*, 1985, **56**, 719.

The electronic mobility in the zintl phase $\text{Yb}_9\text{Mn}_{4.2}\text{Sb}_9$ can be improved by substituting Zn on the Mn site, leading to an improved thermoelectric quality factor.

